

## Valence-orbital-electron momentum distributions for butanone

G. Q. Li, J. K. Deng,\* B. Li, X. G. Ren, and C. G. Ning

*Department of Physics and Key Laboratory of Atomic and Molecular NanoSciences of MOE, Tsinghua University, Beijing 100084, People's Republic of China*

(Received 20 March 2005; revised manuscript received 27 June 2005; published 22 December 2005)

We report here the measurements of the complete valence shell binding energy spectra and the valence-orbital momentum profiles of butanone using the binary ( $e, 2e$ ) electron momentum spectroscopy. The impact energy was 1200 eV plus the binding energy and the symmetric noncoplanar kinematics was used. The experimental momentum profiles of the valence orbitals are compared with the theoretical momentum distributions calculated using Hartree-Fock and density functional theory methods with various basis sets. The experimental measurements are generally described by theoretical calculations except for summed  $4a''$ ,  $15a'$ ,  $3a''$ , and  $14a'$  orbital and summed  $8a'$ ,  $7a'$ , and  $6a'$  orbitals.

DOI: [10.1103/PhysRevA.72.062716](https://doi.org/10.1103/PhysRevA.72.062716)

PACS number(s): 34.80.Gs

### I. INTRODUCTION

Electron momentum spectroscopy (EMS), based on the binary ( $e, 2e$ ) reaction, is now a well-established technique for the investigation of the valence electronic structure of atoms and molecules [1–6]. It is unique in its ability to measure electron momentum profiles of individual molecular orbitals. Experimental momentum profiles are extremely useful for correct assignment of atomic and molecular ionic states and stringent tests of quantum chemical calculations and basis sets. Now a large body of EMS measurements are available for a wide variety of targets such as ethane [7], pharmaceutical amantadine [8], urotropine [9], and ethylene [10]. These results have convincingly shown that the interplay of EMS measurements and high level quantum mechanical calculations provides very detailed information on the binding energy, electronic structure, reactivity, and electron density distributions of electrons in molecules. Furthermore, EMS can provide information relevant to issues of chemical reaction and molecular recognition because electron momentum density is highly sensitive to diffuse parts of the position space wave function [11].

Butanone, also known as methyl ethyl ketone, has a small autoprotolysis constant, relatively high permittivity and dipole moment. On account of these properties it is suitable as a solvent for the determination of weak organic acids and bases, either individually or in mixtures [12]. Butanone is also a solvent of industrial interest for anthracene oxidation [13]. Therefore, the detailed molecular mechanism of butanone is required, including a detailed knowledge of the molecular electron density. Thus far electron momentum spectroscopy is the only experimental technique capable of imaging effectively the valence orbital electron density distributions. In this paper, we report the measurements of the complete valence shell binding energy spectra and the valence-electron momentum profiles of butanone. The experiment was performed at impact energy of 1200 eV plus the binding energy and using symmetric noncoplanar kinematics.

The experimental momentum profile is compared with the Hartree-Fock (HF) and density functional theory (DFT) calculations using different basis sets.

### II. EXPERIMENTAL METHODS AND THEORETICAL CALCULATIONS

In a binary ( $e, 2e$ ) experiment, the scattered and ionized electrons are detected at the same kinetic energies and the same polar angles in symmetric, noncoplanar scattering geometry. In this work, a symmetric noncoplanar, energy dispersive, multichannel EMS spectrometer is used and a detailed description of the spectrometer is given elsewhere [14]. Briefly, two hemispherical electron energy analyzers are mounted on two independent horizontal concentric turntables. The polar angles of both analyzers, in the present work, are kept fixed at  $45^\circ$ . One analyzer turntable is kept in a fixed position while the other is rotated by a computer controlled stepping motor. Each electron energy analyzer accepts a range of kinetic energies from 596 to 604 eV simultaneously, but only those coincident electron pairs with summed energies in the range of  $1200 \pm 3.5$  eV are recorded [14]. The coincidence energy resolution of the spectrometer is measured to be 1.2 eV FWHM. The experimental momentum resolution is estimated to be 0.1 a.u. from a consideration of the argon  $3p$  angular correlation. The sample of butanone (99.9% purity, commercially purchased) is used in measurement without further purification.

EMS cross-section measurements are usually interpreted using the plane wave impulse approximation (PWIA). Considering the binary encounter approximation as well as the target Hartree-Fock approximation (THFA), the triple differential EMS cross section for randomly oriented gas-phase targets can be given [2]

$$\sigma_{\text{EMS}} \propto \int d\Omega |\psi_j(\mathbf{p})|^2, \quad (1)$$

where  $\mathbf{p}$  is the momentum of the target electron prior to knockout and  $\psi_j(\mathbf{p})$  is the one-electron momentum space canonical Hartree-Fock orbital wave function in the neutral

\*Electronic address: [djk-dmp@mail.tsinghua.edu.cn](mailto:djk-dmp@mail.tsinghua.edu.cn)

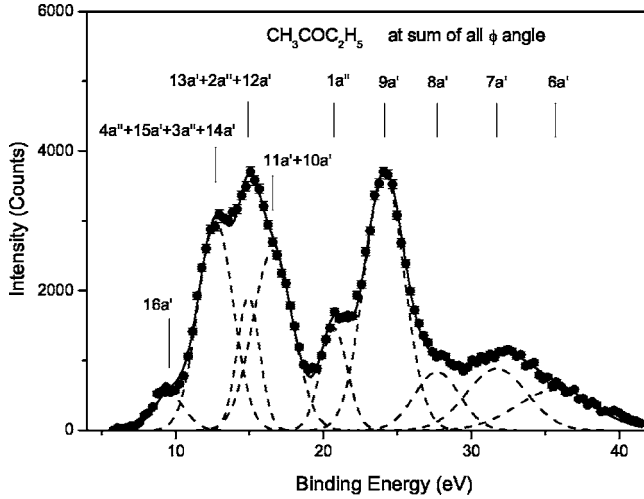


FIG. 1. EMS binding energy spectra of butanone from 6 to 42 eV at sum of all  $\phi$  angles. The dashed lines represent Gaussian fits to the individual peaks and the solid curve is the summed fit.

initial state for the  $j$ th electron that is ionized. The  $\int d\Omega$  represents the spherical average due to the randomly oriented gas phase target. The integral in Eq. (1) is known as the spherically averaged one-electron momentum distribution. To this extent, EMS has the ability to image the electron density in an individual orbital selected according to its binding energies.

The Kohn-Sham density functional theory provides the alternative method to interpret EMS cross section [15]. And the target Kohn-Sham approximation (TKSA) supplies a result similar to Eq. (1) but with the canonical Hartree-Fock orbital replaced by a momentum space Kohn-Sham orbital  $\psi_j^{\text{KS}}(\mathbf{p})$ ,

$$\sigma_{\text{EMS}} \propto \int d\Omega |\psi_j^{\text{KS}}(\mathbf{p})|^2. \quad (2)$$

It should be noted that accounting for electron correlation effects in the target ground state is included in the TKSA via

$$(\text{core})^{10} \underbrace{(6a')^2(7a')^2(8a')^2(9a')^2(1a'')^2}_{\text{inner valence}} \underbrace{(10a')^2(11a')^2(12a')^2(2a'')^2(13a')^2(14a')^2(3a'')^2(15a')^2(4a'')^2(16a')^2}_{\text{outer valence}}.$$

In the ground state, the 40 electrons are arranged in 20 doubly occupied orbitals and the orbitals are either  $a'$  type or  $a''$  type. The valence electrons in butanone are distributed in 15 molecular orbitals. There is no degeneracy in these orbitals. The order of occupation for these valence orbitals comes from our calculations.

To obtain the experimental momentum profiles (XMPs), 11 binding energy spectra over the energy range of 6–42 eV

the exchange correlation potential. A more detailed description of the TKSA-DFT method could be found elsewhere [15].

In the present work, the spherically averaged theoretical momentum profiles have been calculated for the valence orbitals of butanone using PWIA. Details of the calculation methods are described below. The Hartree-Fock and DFT calculations of butanone are carried out by using Eqs. (1) and (2). The Hartree-Fock calculations of the momentum profiles were performed with the basis sets of 6-31G and 6-311++G\*\*. The B3LYP and B3PW91 functionals [16,17] are used for the two DFT calculations, respectively. Three basis sets 6-31G, 6-311++G\*\*, and aug-ccpVTZ are used for the B3LYP and B3PW91 calculations.

The 6-31G basis of Pople and co-workers [18] is a split-valence basis comprised of an inner valence shell of six  $s$ -type Gaussians and an outer valence shell that has been split into two parts represented by three and one primitives, respectively.

The 6-311++G\*\* is an augmented version by Pople *et al.* The outer valence shell is split into three parts and represented by three, one and one primitives. Very diffused  $s$  and  $p$  functions, and spherical  $d$ -type polarization functions are added for carbon atoms, the full set of 6d Cartesian  $d$  functions has been used in the 6-311++G\*\* basis set, and a diffused  $sp$  shell and  $p$ -type polarization function are added for hydrogen atoms [19].

The basis set aug-ccpVTZ was taken from the work of Dunning *et al.* [20]. This basis set used in the present work is actually a truncated form of Dunning's aug-ccpVTZ basis set in which all  $g$  and  $h$  functions have been removed. One  $s$ , one  $d$ , and one  $p$  diffuse functions are added for hydrogen atoms. And one  $d$ , one  $p$ , one  $d$ , and one  $f$  diffuse functions are added for carbon atoms. The full set of 6d Cartesian  $d$  functions has been used.

### III. RESULTS AND DISCUSSIONS

The point group symmetry of butanone is  $C_s$ . According to the molecular orbital theory, the ground state electronic configuration can be written as

were collected at the out-of-plane azimuthal angles  $\phi=0^\circ, 1^\circ, 2^\circ, 3^\circ, 5^\circ, 7^\circ, 9^\circ, 11^\circ, 13^\circ, 15^\circ, \text{ and } 20^\circ$  in a series of sequential repetitive scans. Figure 1 shows the valence shell binding energy spectra of butanone in the range of 6–42 eV summed over all the  $\phi$  angles at 1200 eV impact energy plus the binding energy. The energy scale in Fig. 1 was calibrated with respect to the  $(16a')$ -1 vertical ionization potential from PES data [21]. The spectra in Fig. 1 are fitted with a set of

TABLE I. The ionization energy for butanone.

Orbital	Experimental results			Theoretical orbital energies <sup>a</sup>	
	EMS <sup>a</sup>	PES <sup>b</sup>	PES <sup>c</sup>	HF-6-311++G <sup>**</sup>	B3PW91-6-311++G <sup>**</sup>
16a'	9.56	9.56	9.52	11.10	6.93
4a''		12.26	12.2	13.31	9.63
15a'		12.66	12.6	13.89	10.07
3a'	12.71	13.02	13.0	13.99	10.12
14a'		(13.5)	14.3	14.21	10.13
13a'		14.37	14.8	15.57	11.26
2a''	14.92	(14.9)	15.3	15.90	11.71
12a'		15.34	15.9	17.03	12.23
11a'	16.56	15.97	17.6	17.47	13.09
10a'		(16.8)	18.0	18.04	13.13
1a''	20.70			19.96	14.47
9a'	24.11			23.94	17.70
8a'	27.68			27.27	20.33
7a'	31.72			28.93	21.64
6a'	35.66			38.14	28.94

<sup>a</sup>This work.<sup>b</sup>From Ref. [21].<sup>c</sup>From Ref. [22].

individual Gaussian peaks whose widths are combinations of the EMS instrumental energy resolution and the corresponding Franck-Condon widths derived from high resolution PES data [21]. The dashed lines indicate the fitted Gaussians for individual peaks while the solid line represents the sum. The relative energy values are given by the relative ionization energies determined by high resolution PES. The measured ionization potentials of this work and early PES data [21,22] and the Hartree-Fock and DFT values are compared in Table I. From Table I, we can see that the differences of the theoretical orbital energies obtained from two theoretical calculations are in evidence. The shortcomings of the Kohn-Sham orbital energies as approximate Dyson orbital energies are well known, while the shapes of Kohn-Sham DFT momentum profiles are often in reasonable agreement with experiment. A more detailed assessment of the Kohn-Sham orbitals as approximate Dyson orbitals for the calculation of EMS momentum profiles could be found elsewhere [15].

In the EMS binding energy spectra of Fig. 1, however, only 16a', 1a'', and 9a' orbitals could be clearly identified. The other orbitals could not be identified; some orbitals overlap with one another, which even the high resolution PES could not resolve [21].

Experimental momentum profiles shown in Figs. 2–8 are extracted from the sequentially obtained, angular-correlated binding energy spectra. Various theoretical momentum profiles (TMPs) of the valence orbitals are obtained as described above. The finite experimental momentum resolution ( $\Delta p \sim 0.1$  a.u.) is also folded into the TMPs by using the Gaussian-weighted planar grid method [23]. Experimental data and theoretical values have been placed on a common intensity scale by normalizing the DFT-B3PW91 with aug-ccpVTZ theoretical momentum profiles for Figs. 2–8.

The first peak of butanone, positioned at 9.56 eV in the binding energy spectrum in Fig. 1, is associated with 16a' electrons. The experimental and the theoretical momentum profiles for the 16a' orbital of butanone are shown in Fig. 2. It can be seen from Fig. 2 that the experimental and the theoretical momentum profiles are all “*p-p* type” distribution. However, the theoretical momentum profiles show an interesting feature. The intensity of the second peak is higher than the first peak for calculations using basis sets 6-31G (curves 3, 6, 8), but for the basis sets 6-311++G<sup>\*\*</sup> (curves 2, 5, 7) and aug-ccpVTZ (curves 1, 4), the intensity of the second peak is lower than the first one. It can be concluded from comparing the theoretical calculations with experimen-

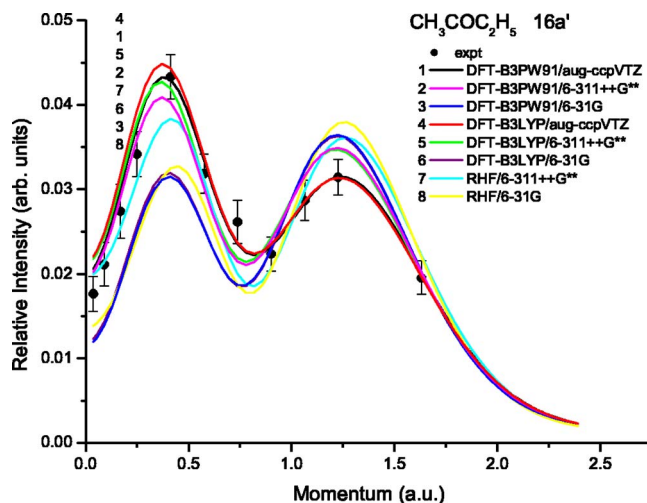


FIG. 2. (Color online) The experimental and calculated momentum distributions for 16a' orbital of butanone.

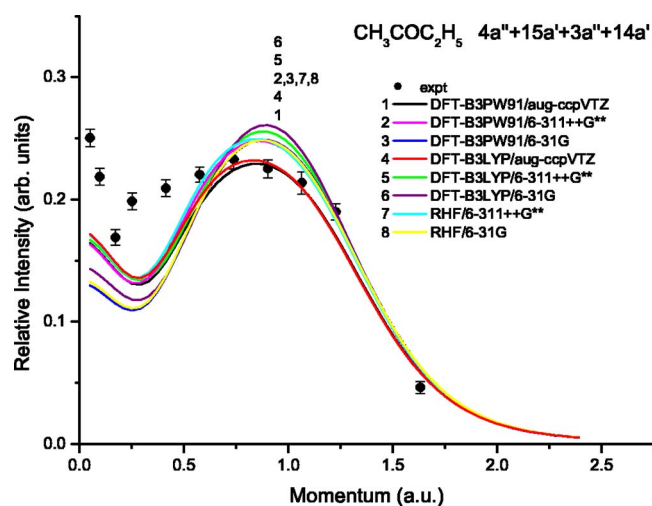


FIG. 3. (Color online) The experimental and calculated momentum distributions for the summed  $4a''$ ,  $15a'$ ,  $3a''$ , and  $14a'$  orbitals of butanone.

tal results in Fig. 2 that momentum profiles calculated using DFT and HF with 6-31G cannot provide a good description for the experimental momentum profile and the intensity distributions are significantly different. Even the HF and DFT calculations at the 6-311++G\*\* level still significantly overestimate the experimental results at momenta above  $\sim 1.0$  a.u., and below 0.5 a.u., the TMP calculated using HF with 6-311++G\*\* underestimate the XMP. This means that the density distributions of the  $16a'$  orbital cannot be described correctly by theoretical calculation either HF or DFT with basis sets 6-311++G\*\* and 6-31G. Figure 2 shows that the B3PW91 and B3LYP calculations with aug-ccpVTZ provide very good quantitative agreement with the EMS measurement. A good description of the XMP by Dunning's correlation consistent basis sets indicates that electron correlation effects are very important for the  $16a'$  orbital, dynamic electron correlated effects must be in-

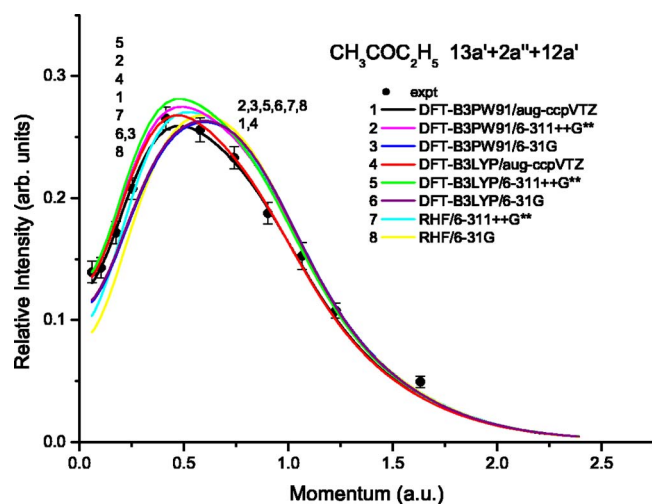


FIG. 4. (Color online) The experimental and calculated momentum distributions for the summed  $13a'$ ,  $2a''$ , and  $12a'$  orbitals of butanone.

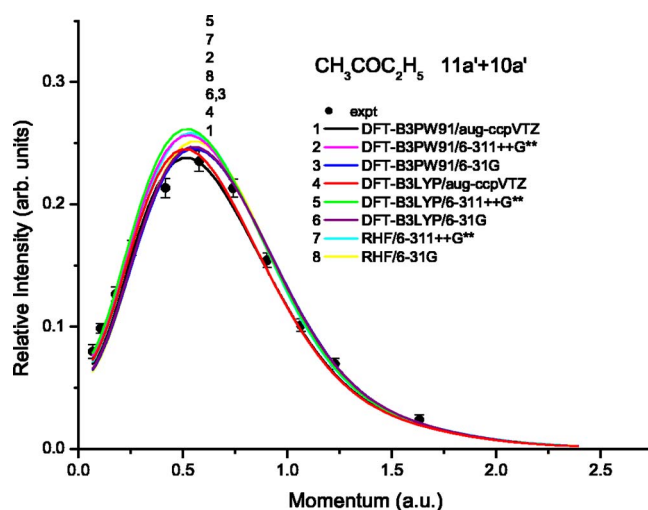


FIG. 5. (Color online) The experimental and calculated momentum distributions for the summed  $11a'$  and  $10a'$  orbitals of butanone.

cluded for quantitative modelling of  $16a'$  electron densities in butanone.

The second peak at 12.71 eV in the binding energy spectrum in Fig. 1 contains contributions from the  $4a''$ ,  $15a'$ ,  $3a''$ , and  $14a'$  orbitals.  $4a''$ ,  $15a'$ ,  $3a''$ , and  $14a'$  orbitals are not well separated experimentally due to their small energy separations. Therefore, summed momentum profiles of the  $4a''$ ,  $15a'$ ,  $3a''$ , and  $14a'$  orbitals are discussed for comparison between experiment and theory. The summed momentum profiles have “*s-p* type” distributions as indicated in Fig. 3. The summed experimental profiles are well fitted by B3PW91 and B3LYP calculations with aug-ccpVTZ (curves 1, 4) in the momentum region above 0.6 a.u., and other four DFT calculations (curves 2, 3, 5, 6) and two HF calculations (curves 7, 8) overestimate the intensity in this region. There is a significant discrepancy between theoretical calculations and experimental data below the momentum of 0.6 a.u. and

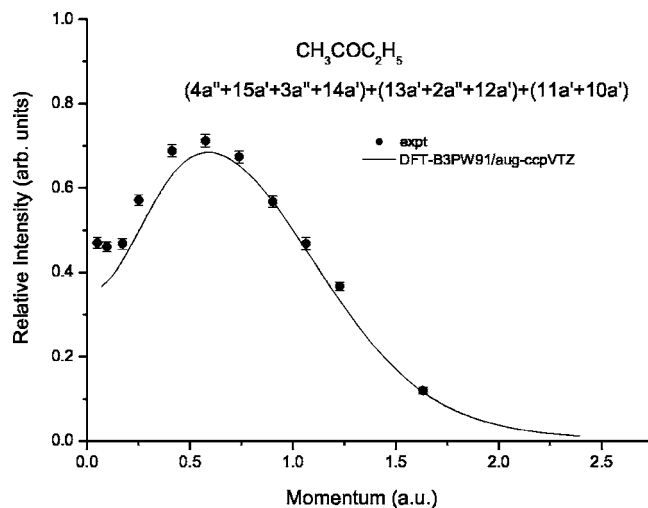


FIG. 6. The experimental and calculated momentum distributions for the summed ( $4a''$ ,  $15a'$ ,  $3a''$ ,  $14a'$ ), ( $13a'$ ,  $2a''$ ,  $12a'$ ), and ( $11a'$ ,  $10a'$ ) orbitals of butanone.

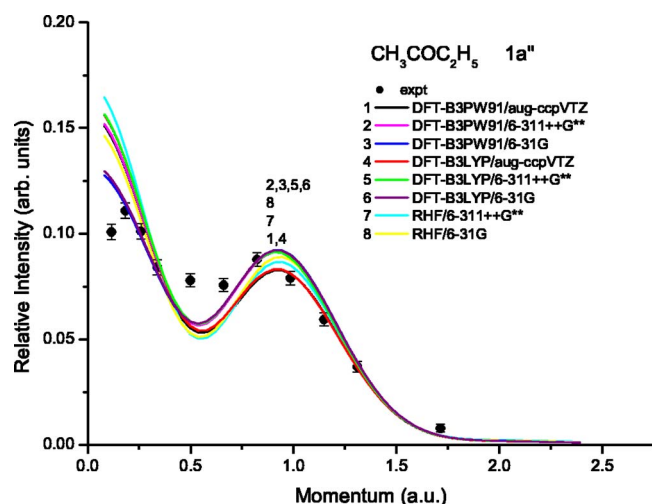


FIG. 7. (Color online) The experimental and calculated momentum distributions for  $1a''$  orbital of butanone.

all theoretical calculations underestimate the experimental intensity, although slight improvement is obtained by the DFT calculation. The discrepancy between experiment and theory in the low momentum region is probably due to inaccuracies in the Gaussian fitting procedures since the nearby two ionization peaks are very close, and some intensity of the third peak could leak into the second peak in the low momentum range. Another possible source for the discrepancy in the low momentum range could be considered the distorted wave effects. Unfortunately at present the distorted wave effects cannot be calculated for molecules. A possible clue for understanding the observations here may be found in the Cr  $3d$  ionization process [24], which is known as the only case where distorted wave effects in the low momentum region have been verified by theoretical calculations. Brion *et al.* [24] proposed in an interpretive model that such unexpected “turn up” is due to the high angular momentum effects and the even-parity nature of an atomic  $d$  orbital. Furthermore, they suggested that similar effects may occur for

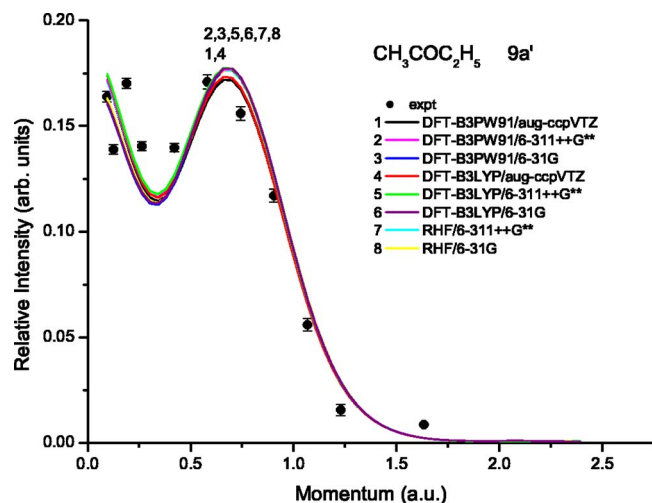


FIG. 8. (Color online) The experimental and calculated momentum distributions for  $9a'$  orbital of butanone.

atomic  $d$ - or  $\pi^*$ -like molecular orbitals in diatomic and small polyatomic molecules that exhibit gerade type symmetry [25]. Clearly, the  $4a''$  orbital of butanone is of gerade type and the discrepancy of the low momentum region may be caused by the distorted wave effects of this orbital. Recently, Ren *et al.* attempted to support this suggestion by researching the  $1b_{3g}$  orbital of ethylene [10].

The third peak of butanone at 14.92 eV in the binding energy spectrum in Fig. 1 contains contributions from the  $13a'$ ,  $2a''$ , and  $12a'$  orbitals. Summed experimental and theoretical momentum profiles for the  $13a'$ ,  $2a''$ , and  $12a'$  orbitals are shown in Fig. 4. The summed momentum profile is a  $p$ -type distribution. It can be seen from Fig. 4 that the theoretical calculations are almost the same except for B3PW91 and B3LYP calculations with basis set aug-ccpVTZ (curves 1, 4) in the momentum region above 0.7 a.u. and there is some discrepancy in the momentum region below 0.7 a.u. The comparison between the summed experimental data and the summed theoretical calculations in Fig. 4 shows that B3PW91 and B3LYP calculations with aug-ccpVTZ provides a better fit to the experimental data. This suggests that electron correlation effects are important for this orbital. DFT and HF with 6-31G and 6-311++G\*\* basis sets cannot provide a good description of the experimental data.

The fourth peak of butanone at 16.56 eV in the binding energy spectrum in Fig. 1 contains contributions from the  $11a'$ , and  $10a'$  orbitals. Summed experimental and theoretical momentum profiles for the  $11a'$  and  $10a'$  orbitals are shown in Fig. 5. The summed momentum profile is a  $p$ -type distribution. It can be seen from the comparison in Fig. 5 that the theoretical momentum profiles are almost the same except for B3PW91 and B3LYP calculations with aug-ccpVTZ (curves 1, 4) in the momentum region above 0.75 a.u., and the theoretical momentum profiles are close in the momentum region below 0.3 a.u. There are some discrepancies in the momentum region between 0.3 a.u. and 0.7 a.u. The summed theoretical calculations reproduce the experimental momentum profile.

Experimental data and theoretical momentum profile obtained by DFT-B3PW91 with aug-ccpVTZ in Figs. 3–5 have been summed, and shown in Fig. 6. The summed theoretical momentum profile gives a very reasonable description for the summed experimental data in the momentum range above 0.6 a.u. and significantly underestimates the experimental data in the momentum range below 0.6 a.u. This shows that the discrepancy between experiment and theory below 0.6 in Fig. 3 is not mainly due to a possible error in the curve fitting and deconvolution procedures and there are other sources to cause the significant discrepancy in the low momentum region. A possible source could be that the distorted wave effect causes a significant discrepancy in the momentum region.

The experimental and theoretical momentum profiles for the inner-valence orbitals of butanone are shown in Figs. 7–9, respectively. It should be noted that the energy positions and widths for the inner orbitals, used in the deconvolution procedure, are not based on published photoelectron spectra, but rather on an estimate from the present molecular orbital calculations and the fitting quality of the individual binding energy spectra (Fig. 1) collected at different  $\phi$  angles. The

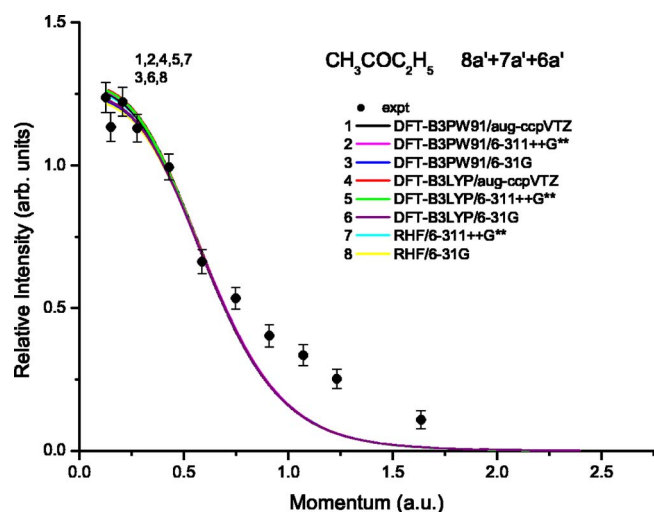


FIG. 9. (Color online) The experimental and calculated momentum distributions for the summed  $8a'$ ,  $7a'$ , and  $6a'$  orbitals of butanone.

first inner valence of butanone is  $1a''$  orbital, peaked at 20.70 eV in the binding energy spectrum in Fig. 1. The experimental and theoretical momentum profiles for the  $1a''$  orbital are shown in Fig. 7. The theoretical momentum profiles show the “ $s$ - $p$  type” momentum distribution. There are discrepancies between the DFT and HF calculations at the momentum region below 1.2 a.u. The comparison between the experimental data and theoretical calculations in Fig. 7 shows that the B3PW91 and B3LYP calculations can describe the experimental data except the momentum region between 0.4 a.u. and 1.0 a.u. and below 0.25 a.u. All theoretical calculations underestimate the experimental data in the momentum region between 0.4 a.u. and 1.0 a.u. Similar phenomena of the “ $s$ - $p$  type” momentum distribution have been observed in the ( $e$ ,  $2e$ ) research of  $3a_{1g}$  orbital of ethane [7]. It appears that an overly spatially diffuse orbital has resulted from the DFT calculations adding diffuse functions in the low momentum region (curves 1, 2, 4, 5). The second inner-valence orbital is the  $9a'$  orbital positioned at 24.11 eV in the binding energy spectrum in Fig. 1. The experimental and theoretical momentum profiles for the  $9a'$  orbital are shown in Fig. 8. The theoretical momentum profiles show the  $s$ - $p$  type momentum distribution. It can be seen from Fig. 8 that the shapes and intensities obtained by DFT and HF calculations are very similar. This means that the choice of the basis sets is not important for the  $9a'$  orbital. The theoretical momentum profiles cannot well describe the experimental data. It can be seen from Fig. 1 that the  $9a'$  orbital can be clearly identified. The discrepancy between experiment and theory in Fig. 8 is not due to a possible error in the curve fitting and the deconvolution procedures and may be caused by the final state correlation effect. Weigold *et al.* suggest that the inner valence region often shows complex

structure, generally the result of final state correlation effect [2]. The experimental and theoretical momentum profiles of the  $8a'$ ,  $7a'$ , and  $6a'$  orbitals are summed because of the peaks of the  $8a'$ ,  $7a'$ , and  $6a'$  orbitals are wide and the counts are relatively small (see Fig. 1). The summed momentum profiles are shown in Fig. 9. The summed theoretical momentum profiles show the “ $s$ -type” distribution. The theoretical momentum profiles obtained by DFT and HF calculations are the same at the momentum region above 0.5 a.u., with only a slight discrepancy at the momentum region below 0.5 a.u. This means that the choice of the basis sets is not important for this orbital. The comparison between the experimental data and theoretical calculations in Fig. 9 shows that theoretical calculations generally describe the experimental data below 0.8 a.u. However, there is a discrepancy between theoretical calculations and experimental data above the momentum of 0.8 a.u., and the theoretical calculations underestimate the experimental intensity. The ionization processes of inner valence have been split into higher energy satellite “poles” due to the final state correlation effect. The pole strength cannot be estimated because some orbitals cannot be identified clearly. The experimental data in Fig. 9 may contain the satellite intensity of  $1a''$  and  $9a'$  due to the final state correlation effect. The discrepancy between theoretical calculations and experimental data may be caused by the final state correlation effect.

#### IV. SUMMARY

In summary, the valence shell binding energy spectra and the momentum profiles of butanone were measured by using the binary ( $e$ ,  $2e$ ) electron momentum spectrometer. The experimental momentum profiles are compared with the theoretical momentum distributions calculated using Hartree-Fock and density functional theory methods with various basis sets. The binding energies are given in Table I. The experimental measurements are generally described by theoretical calculations except for summed  $4a''$ ,  $15a'$ ,  $3a''$ , and  $14a'$  orbitals and summed  $8a'$ ,  $7a'$ , and  $6a'$  orbitals. A significant discrepancy between theoretical calculations and experimental data is observed for summed  $4a''$ ,  $15a'$ ,  $3a''$ , and  $14a'$  orbitals below the momentum of 0.6 a.u. due to possible distorted wave effects of  $4a''$  orbital. In general the experimental momentum profiles are well described by DFT calculations using B3PW91 and B3LYP functionals with aug-ccpVTZ basis set.

#### ACKNOWLEDGMENTS

This project was supported by the National Natural Science Foundation of China under Grants Nos. 19854002, 19774037, and 10274040 and the Research Fund for the Doctoral Program of Higher Education under Grant No. 1999000327.

- [1] I. E. McCarthy and E. Weigold, *Rep. Prog. Phys.* **91**, 789 (1991), and references therein.
- [2] E. Weigold and I. E. McCarthy, *Electron Momentum Spectroscopy* (Kluwer Academic/Plenum, New York, 1999).
- [3] C. E. Brion, in *The Physics of Electronic and Atomic Collisions*, edited by T. Anderson *et al.* (American Institute of Physics Press, New York, 1993), p. 350.
- [4] C. E. Brion, G. Cooper, Y. Zheng, I. V. Litvinyuk, and I. E. McCarthy, *Chem. Phys.* **270**, 13 (2001).
- [5] K. T. Leung, in *Theoretical Models of Chemical Bonding*, edited by Z. B. Maksic (Springer-Verlag, Berlin, 1991), p. 339.
- [6] A. O. Bawagan, *et al.*, *Chem. Phys.* **113**, 19 (1987).
- [7] J. K. Deng *et al.*, *J. Chem. Phys.* **117**, 4839 (2002).
- [8] I. V. Litvinyuk, Y. Zheng, and C. E. Brion, *Chem. Phys.* **261**, 289 (2000).
- [9] I. V. Litvinyuk *et al.*, *Chem. Phys.* **263**, 195 (2001).
- [10] X. G. Ren, C. G. Ning, J. K. Deng, S. F. Zhang, G. L. Su, F. Huang, and G. Q. Li, *Phys. Rev. Lett.* **94**, 163201 (2005).
- [11] D. L. Cooper and N. L. Allan, *J. Am. Chem. Soc.* **114**, 4773 (1992).
- [12] R. P. Mihajlovic, V. M. Joksimovic, and Lj. V. Mihajlovic, *Talanta* **61**, 331 (2003), and references therein.
- [13] E. A. Cepeda and J. M. Diaz, *Fluid Phase Equilib.* **121**, 267 (1996), and references therein.
- [14] J. K. Deng *et al.*, *J. Chem. Phys.* **114**, 882 (2001).
- [15] P. Duffy, D. P. Chong, M. E. Casida, and D. R. Salahub, *Phys. Rev. A* **50**, 4707 (1994), and references therein.
- [16] J. P. Perdew and Y. Wang, *Phys. Rev. B* **33**, R8800 (1986), and reference therein.
- [17] A. D. Becke, *Phys. Rev. A* **38**, 3098 (1988).
- [18] R. Krishnan, M. J. Frisch, and J. A. Pople, *J. Chem. Phys.* **72**, 4244 (1980).
- [19] M. J. Frisch, J. A. Pople, and J. S. Binkley, *J. Chem. Phys.* **80**, 3265 (1984), and reference therein.
- [20] D. E. Woon and T. H. Dunning, Jr., *J. Chem. Phys.* **99**, 1914 (1993), and reference therein.
- [21] K. Kimura, S. Katsumata, Y. Achiba, T. Yamazaki, and S. Iwata, *Handbook of HeI Photoelectron Spectra of Fundamental Organic Molecules* (Japan Scientific Society, Tokyo, 1981).
- [22] Wing-Cheung Tam, D. Yee, and C. E. Brion, *J. Electron Spectrosc. Relat. Phenom.* **4**, 77 (1974).
- [23] P. Duffy *et al.*, *Chem. Phys.* **159**, 347 (1992).
- [24] C. E. Brion, Y. Zheng, J. Rokle, J. J. Neville, I. E. McCarthy, and J. Wang, *J. Phys. B* **31**, L223 (1998).
- [25] J. Rokle, Y. Zheng, C. E. Brion, Z. Shi, S. Wolfe, and E. R. Davidson, *Chem. Phys.* **244**, 1 (1999).